

Technical University of Munich



HORYZN



Institute of Flight System Dynamics



# Design and Analysis of a multipurpose Landing Gear system for HORYZN's UAV for the GoAERO competition

—

Entwurf und Analyse eines multifunktionalen Landegestells für das  
HORYZN UAV für den GoAERO-Wettbewerb

Engineering Project

Authors: Adrián Reigosa Rico and Jarom Schlien

Matriculation Number: 03776052, 03768407

Supervisor: M.Sc. Michael Bachfischer

Examiner: Prof. Dr.-Ing. Florian Holzapfel

2025-07-21

## Statutory Declaration

We, Adrián Reigosa Rico and Jarom Schlien, declare on oath towards the Institute of Flight System Dynamics of Technical University of Munich, that we have prepared the present Engineering Project independently and with the aid of nothing but the resources listed in the bibliography.

This Engineering Project has neither as-is nor similarly been submitted to any other university.

Garching, 2025-07-21

Adrián Reigosa Rico and Jarom Schlien

**Abstract**

*The HORYZN student initiative at the Technical University of Munich (TUM) is developing an autonomous eVTOL ambulance for the 2027 GoAERO Prize. This Engineering Project documents the design, analysis and prototype manufacturing of a multipurpose Landing Gear System (LGS) for the flier. The design followed over 40 design requirements, including landing on multiple surfaces like a 12° slope, sand, and water; under an LGS weight limit of 20 kg at a maximum take off mass of 380 kg in a landing scenario of a 0.46 m drop.*

*The work compares materials and LGS configurations to select an aluminium 7075 skid type, since it behaves as a leaf spring, capable of absorbing energy with deflection. After defining the load cases and checking the static stability, the creation and analysis of the LGS model is performed: Firstly, a parametric LGS design with CATIA V6 is created. Secondly, an optimisation method investigates the best LGS geometry and cross-section. Finally, the Finite Element Analysis is conducted on the optimum CAD to evaluate its feasibility with failure analysis. The analysis yields a hollow rectangular cross-section 130 x 18 mm with 3 mm thickness, capable of handling a 31 kN load with a 40 cm crossbeam deflection while fulfilling all the requirements.*

*The report mentions that glass fiber reinforced plastics might be a feasible alternative due to their high specific strength. It is noted that there is a lack of literature covering glass fiber composite LGS.*

**Kurzfassung**

*Die studentische Initiative HORYZN an der Technischen Universität München (TUM) entwickelt derzeit eine autonome eVTOL-Rettungsdrohne für den GoAERO Prize 2027. Dieses Engineering-Projekt dokumentiert die Konstruktion, Analyse und Prototypenfertigung eines multifunktionalen Landegestells (LGS) für das Fluggerät. Das Design erfüllt über 40 Anforderungen, darunter Landungen auf unterschiedlichen Oberflächen wie 12°-Schräge, Sand und Wasser, bei einem LGS-Gewichtslimit von 20kg und einer maximalen Startmasse von 380kg aus 0.46m Fallhöhe.*

*Basierend auf Materialvergleichen wurde ein Skid-LGS aus Aluminium 7075 gewählt, da es wie eine Blattfeder wirkt und Energie durch Verformung aufnimmt. Nach Definition der Lastfälle und Prüfung der Stabilität wurde ein parametrisches Modell in CATIA V6 entworfen, optimiert und mittels Finite-Elemente-Methode auf Stabilität geprüft. Die optimale Lösung: ein hohles Rechteckprofil (ca. 130×18mm, 3mm Wandstärke), das 31kN Last bei 40cm Durchbiegung trägt.*

*Der Bericht schließt mit dem Hinweis, dass Glasfaser verstärkte Kunststoffe, aufgrund ihrer hohen spezifischen Stärke, eine mögliche Alternative zu Aluminium darstellen könnten. Es wird darauf verwiesen, dass Glasfaser-Komposit-LGS kaum in der Literatur behandelt werden.*

## Table of Contents

List of Figures	iv
List of Tables	v
Table of Acronyms	vi
Table of Symbols	vii
1. Introduction	1
1.1. Motivation: HORYZN and the GoAERO competition . . . . .	1
1.2. State of the Art . . . . .	1
2. Design and analysis	3
2.1. Definition of Requirements: GoAERO, HORYZN and Certification . . . . .	3
2.1.1. GoAERO Fly-Off Rulebook relevant requirements: . . . . .	3
2.1.2. Certification CS-27 relevant requirements: . . . . .	5
2.1.3. HORYZN relevant requirements . . . . .	7
2.2. Material considerations . . . . .	8
2.3. Comparison of Landing Gear configurations . . . . .	8
2.4. Static stability in slope . . . . .	9
2.4.1. Sliding angle . . . . .	9
2.4.2. Pitch over angle . . . . .	9
2.4.3. Roll over angle . . . . .	9
2.5. Definition of Load Cases . . . . .	10
2.6. Analysis: iteration of cross-sections and load cases . . . . .	11
2.6.1. CAD model . . . . .	11
2.6.2. Optimisation Process . . . . .	11
2.6.3. FEA of the optimal CAD model . . . . .	16
2.6.4. Failure Analysis . . . . .	17
2.6.5. Application of Strength and Stability Analysis . . . . .	21
2.7. Manufacturing of scaled prototype . . . . .	22
3. Conclusion and Outlook	23
References	I
A. Appendix: Additional Material	III

## List of Figures

2-1.	Sketch of the static stability in slope sketch . . . . .	10
2-2.	Master Assembly of the LGS . . . . .	11
2-3.	Thin Box/ Thin-Walled Rectangular CS . . . . .	15
2-4.	LG Stick Model . . . . .	16
2-5.	LG Visualisation . . . . .	16
2-6.	RBE2 Element Bow . . . . .	17
2-7.	RBE2 Element Skid . . . . .	17
2-8.	End Fixity Coefficient . . . . .	18
2-9.	$b_i$ of different cross sections . . . . .	19
2-10.	Deformation, Rectangular . . . . .	21
2-11.	Deformation, I-Beam . . . . .	21
2-12.	Scaled prototype . . . . .	22
A-1.	Competitor Study . . . . .	III

## List of Tables

2-1.	GoAERO Fly-Off Rulebook relevant requirements . . . . .	3
2-1.	GoAERO Fly-Off Rulebook relevant requirements (Continued) . . . . .	4
2-1.	GoAERO Fly-Off Rulebook relevant requirements (Continued) . . . . .	5
2-2.	Certification CS-27 relevant requirements . . . . .	5
2-2.	Certification CS-27 relevant requirements (Continued) . . . . .	6
2-3.	HORYZN relevant requirements . . . . .	7
2-4.	Overview of Load Cases . . . . .	10
2-5.	Design requirements and constants . . . . .	11
2-6.	Direct input variables and their definitions . . . . .	12
2-7.	List of constraints . . . . .	12
2-8.	List of system variables . . . . .	12
2-9.	Maximum applied stress per CS . . . . .	15
2-10.	thin-bow CS optimised dimensions . . . . .	15
2-11.	Critical Stresses of LG Sections . . . . .	21
A-1.	Material comparison table [13] . . . . .	III

## Table of Acronyms

Acronym	Description
Al	Aluminium
CAD	Computer-Aided Design
CFRP	Carbon Fiber Reinforced Plastic
COG	Centre Of Gravity
CS	Cross-Section
EAR	Energy Absorption Ratio
EP	Engineering Project
eVTOL	Electric Vertical Take-Off and Landing aircraft
FEA	Finite Element Analysis
FSD	Institute of Flight System Dynamics
GA	GoAERO competition
GFRP	Glass Fiber Reinforced Plastic
HZ	HORYZN
LC	Load Case
LG	Landing Gear
LGS	Landing Gear System
MFC	Metal Forming and Casting Chair
MTOM	Maximum Take-Off Mass
MTOW	Maximum Take-Off Weight
OZ	Operating Zone
RBE2	Rigid Body Element 2
SPC	Single Point Constraint
STEP	Standard for the Exchange of Product Data
TUM	Technical University of Munich
UAV	Unmanned Aerial Vehicles
US	United States of America

## Table of Symbols

### Latin Letters

Symbol	Description
$A$	Cross-Section Area
$b$	Width
$c$	End Fixity Coefficient
$E$	Young's Modulus
$F$	Force
$g$	Gravitational acceleration
$h$	Centre of gravity height
$I$	Second Moment of Area
$K$	Element Support Factor
$L$	Beam/Column Length
$LL$	Limit Load
$l$	Centre of gravity length
$m$	Flyer mass
$N$	Normal force
$r$	Radius of Gyration
$RF$	Reserve Factor
$SF$	Safety Factor
$t$	thickness
$UL$	Ultimate Load
$w$	Centre of gravity width
$x$	Coefficient for Calculation of Critical Stress Factor

### Greek Letters

Symbol	Description
$\alpha$	Critical Stress Factor
$\lambda$	Column Slenderness
$\sigma$	Stress
$\mu$	Friction Coefficient
$\theta_{crit}$	Critical static stability angle

### Indices

Symbol	Description
$s$	static
$fric$	friction



## 1. Introduction

### 1.1. Motivation: HORYZN and the GoAERO competition

HORYZN (HZ) is a student initiative at TUM founded in 2019 that designs, builds and flies Unmanned Aerial Vehicles (UAV). It has developed plenty of models, highlighting Kolibri or Frankenstein, focused on transporting and deploying a defibrillator to inaccessible areas when necessary.

The next challenge that HZ has decided to face is to participate in the renowned United States of America (US)-based GoAERO competition (GA), where an autonomous Electric Vertical Take-Off and Landing aircraft (eVTOL) ambulance is to be developed, capable of transporting a 57 kg manikin in different environments. Many universities worldwide are taking part, which further powers the motivation of the circa 70 students in the team.

In this context, the topic of this Engineering Project arose: the design, modelling and analysis of a polyvalent LGS for HZ's eVTOL for the GA that fulfils the competition, organisation and some certification requirements while balancing safety, strength, low weight and innovation.

This engineering project was developed in collaboration with HZ and the TUM Institute of Flight System Dynamics (FSD) Chair, which has long supported HZ. May the authors' gratitude to both organisations be noted.

### 1.2. State of the Art

While the design of an eVTOL is a relatively novel concept, the development of a landing gear is a well-researched one. In particular, skid-type LGS are attractive due to their simplicity, low weight, low maintenance, and good energy absorption characteristics. Starting the Engineering Project (EP) with a strong literature background was important so as to consider multiple solutions and have a sense of what is feasible and what is not.

Regarding the LGS configuration, Ding et al. [6] found that among skid-type LGS, the bow-style has the best crashworthiness performance in an emergency landing scenario with a sink velocity of 9.1 m/s compared to strut, arc and oct styles. The study measured the kinetic energy difference before and after impact to measure the Energy Absorption Ratio (EAR). While the bow style showed the best EAR, it had a higher weight because the crossbeam crosses through the fuselage, unlike the other styles. However, as the other styles are directly connected to the fuselage, the fuselage frame should be strengthened in compensation, adding weight.

Material choice is critical for both structural integrity and weight efficiency. Kumar et al. [11] supported the Aluminium (Al) 7075 Alloy as a material for skid-type LGS applications, over steel, titanium and composites, after comparing their material properties and their behaviour under Finite Element Analysis (FEA).

Beyond LGS geometry and material, several studies have addressed numerical analysis approaches. Airoldi et al. [2] developed a numerical model based on multibody optimisation to design a skid-type LGS analysing its dynamic landing behaviour, and concept proofed with drop testing. Élie-dit-Cosaque et. al. [7] proposed a methodology to simulate the landing scenarios of a skid-type LGS in FEA while taking into account the material history after the manufacturing and bending process, which induces residual stresses into the beams. Despite a rich literature, it is possible to identify gaps in it. Often ignored in prior studies, Mikhailov et. al. [14] assessed the second landing impact at skid-type LGS, including it in a model for rotary-wing aircraft landings. They concluded that accounting for this second impact, which induces significant stresses into the structure, significantly improves accuracy in the models, with an error within 10% of experimental results.

Additionally, landing on inclined or uneven surfaces introduces further complexity, which is important to consider. Ahsaei et al. [1] recently addressed this issue by performing a full-scale analysis of a skid-type, Aluminium 7075 Alloy-made LGS landing impact at different roll-attitude angles or surface slopes of 0, 5, 10, 20 and 30 degrees. They concluded that the highest stress happens at 0 degrees and the highest force and acceleration at 10 degrees.

All in all, these studies served as a basis for the outline of the LGS, providing valuable insight into the design process, including the definition of conservative load cases at varied landing situations, and supporting the choice of both the material Al 7075 and the skid-type LGS configuration.

## 2. Design and analysis

### 2.1. Definition of Requirements: GoAERO, HORYZN and Certification

Within the Fly-Off Rulebook [9] provided by GA, the missions and requirements of the competition were defined, which serve as a basis for the design of the LGS. Considering **REQ-LG-GA-14**, the CS-27 (Certification for Small Rotorcraft) [4] was used as a design guideline for the LGS, noting that the required certificate from airworthiness is a more straightforward process than the certification of an aircraft itself. Furthermore, more requirements were defined by HZ (e.g., the weight limit specified by the propulsion team). In total, three missions are to be completed by the flier on the final fly-off of GA:

1. Productivity mission: the ability to transport the flyer using a US-highway legal vehicle, quick deployment, and a total 567 kg payload (manikin, rebars and sandbags) transport in several flights following a trajectory under 90 minutes must be demonstrated.
2. Adversity mission: the most relevant to the design of the LGS. The ability to land in 6 complex environments under 30 minutes of flight with the manikin onboard, touching down for two contiguous minutes on each surface, is to be demonstrated. These are a hard surface, a loose dry sand surface, a 12-degree slope surface, a 0.5 m deep pool with rainfall, a hard surface with strong winds, and an unknown surface with obstacles.
3. Manoeuvring mission: the ability to tightly manoeuvre while avoiding obstacles, flying a pre-defined course, is to be demonstrated.

Points are awarded to each team following evaluation criteria for each mission.

On the following, the requirements and challenges influencing the LGS design are presented, where the coloured ones are the most critical.

#### 2.1.1. GoAERO Fly-Off Rulebook relevant requirements:

Table 2–1.: GoAERO Fly-Off Rulebook relevant requirements

Req. ID.	Title	Definition
REQ-LG-GA-01	Operational Area	The flyer, including the transport vehicle, shall be deployable within an operational area shaped as a trapezoid, measuring 30 m in length, 1.5 m in width at the narrow end closest to the end line, and 9 m at the farthest end.
Continued on next page		

**Table 2–1.: GoAERO Fly-Off Rulebook relevant requirements (Continued)**

Req. ID.	Title	Definition
REQ-LG-GA-02	Productivity Mission	The flyer shall carry a total payload of at least 567 kg in 90 minutes. The payload can consist of up to 12 rebars (2.8 kg per piece), up to three sandbags (18.2 kg per piece), one manikin (57 kg) or any combination of these.
REQ-LG-GA-03	Container Transport Limits	The flyer, operating crew, and all equipment shall be transported inline with US highway limitations, limiting the size to a length of 5.90 m, a width of 2.35 m and a height of 2.39 m.
REQ-LG-GA-04	Repeatability of Payload Transportation	The flyer shall be able to perform a sufficient number of round-trips (including landing, loading, unloading and flying) within 90 minutes, with a minimum of 567 kg ferried weight.
REQ-LG-GA-05	Landing on Hard Surface	The flyer shall be able to land on a hard surface of 7.6 m x 15 m.
REQ-LG-GA-06	Landing on Loose Dry Sand	The flyer shall be able to land on loose dry sand in an area of 3.7 m x 3.7 m, with low visibility.
REQ-LG-GA-07	Landing on an Inclined Surface	The flyer shall be able to land on a 12-degree inclined area of 3.4 m x 3.4 m with carpet, leading to a maximum height at the end of the ramp of 70 cm.
REQ-LG-GA-08	Landing on a Pool	The flyer shall be able to touch or pop a balloon floating anchored, freely moving in a radius of 1.8 m, on a pool with a diameter of 7.3 m and a depth of 0.5 m.
REQ-LG-GA-9	Landing during Strong Wind	The flyer shall be able to land on a hard surface of 4.6 m x 4.6 m with strong, non-uniform wind currents up to $11 \text{ m} \cdot \text{s}^{-1}$ .
REQ-LG-GA-10	Landing in an Unknown Area	The flyer shall be able to detect obstacles within an 18m x 7.6m box, of 0.9 m height, while in landing mode, with a minimum free landing area with a hard surface of 4.6 m diameter.
REQ-LG-GA-11	Payload damage	The payload shall stay intentionally undamaged during all missions.
Continued on next page		

Table 2–1.: GoAERO Fly-Off Rulebook relevant requirements (Continued)

Req. ID.	Title	Definition
REQ-LG-GA-12	Takeoff definition	To be considered as taken off, no part of the aircraft shall be in physical contact with the Operating Zone (OZ).
REQ-LG-GA-13	Landing definition	To be considered as landed, a load-bearing part of the aircraft shall be in contact with the OZ. All parts, components and assemblies shall remain intact.
REQ-LG-GA-14	Certification requirement	To qualify for participation in the GA Fly-Off, an aircraft shall have a registration and an <b>airworthiness certificate</b> by the authorities.

### 2.1.2. Certification CS-27 relevant requirements:

Table 2–2.: Certification CS-27 relevant requirements

Req. ID.	Title	Definition
REQ-LG-CS27-01	Safety factor	A SF of 1.5 shall be used.
REQ-LG-CS27-02	Ultimate Load	The UL shall be equal to the SF times the LL.
REQ-LG-CS27-03	Landing conditions	The rotorcraft shall land with no excessive vertical acceleration, bounce, nose over, ground loop, or water loop, and without exceptional piloting skill or exceptionally favourable conditions.
REQ-LG-CS27-04	Inertia forces	All loads shall be placed in equilibrium with inertia forces.
REQ-LG-CS27-05	Yielding	The structure should support the limit loads without permanent deformation.
REQ-LG-CS27.305-06	Static Test	The structure shall resist ULs in a static test for 3 seconds.
REQ-LG-CS27-07	External loads	The following external loads shall be considered for structural design: Bending moment, shear, torque, etc.
REQ-LG-CS27-08	Internal loads	The following internal loads shall be considered for structural design: strains, stresses, etc.
REQ-LG-CS27-09	Structure concepts	The following structural design concepts shall be considered: details, geometry, structural arrangements, load paths, etc.

Continued on next page

**Table 2–2.: Certification CS-27 relevant requirements (Continued)**

Req. ID.	Title	Definition
REQ-LG-CS27-10	Material	Material deformations, deflection, stress level, and test experience shall be considered.
REQ-LG-CS27-11	Ground loads	The following assumptions shall be made for landing cases to determine the weight, Centre Of Gravity (COG) and load factor $n_z$ : the aircraft is a rigid body, Maximum Take-Off Mass (MTOM) as mass, rotor lift through COG up to two thirds of weight, shock absorbers in the most critical position.
REQ-LG-CS27-12.1	Landing with skids	Structural yielding of elastic spring members under limit loads is acceptable.
REQ-LG-CS27-12.2	Landing with skids	The gear shall be tested in its most critically deflected position.
REQ-LG-CS27-12.3	Landing with skids	Ground reactions shall be rationally distributed along the bottom of the skid tube.
REQ-LG-CS27-13.1	Skid level landing: Vertical loads	Both skids shall be assumed to touch the ground, and vertical reactions shall be considered.
REQ-LG-CS27-13.2	Skid level landing: Horizontal loads	Vertical ground reactions shall be combined with a horizontal axial drag reaction of 50% of the vertical reaction at ground.
REQ-LG-CS27-13.3	Skid level landing: Side loads	Vertical ground reactions shall be combined with horizontal side shear loads of 25% of their value. Unbalanced moments are assumed to be resisted by angular inertia.
REQ-LG-CS27-14	One skid landing	The vertical load on the ground contact side shall be the same as that obtained on that side in the condition of two skids touching the ground level landing. The Maximum Take-Off Weight (MTOW) is considered for one skid.
REQ-LG-CS27.725-15	Shock absorption drop test	The Landing Gear (LG) shall resist a drop test, ensuring reserve energy absorption capacity of 0.46 m or a sink speed of $3 \text{ m} \cdot \text{s}^{-1}$ at impact. The formula for computing the limit inertia load factor is given by the certification agency [4].
REQ-LG-CS27.562-16	Lumbar Force	The maximum compressible load measured between the pelvis and the lumbar column of the test dummy shall not exceed 6674 N.

### 2.1.3. HORYZN relevant requirements

Table 2–3.: HORYZN relevant requirements

Req. ID.	Title	Definition
REQ-LG-HZ-01	Regulatory Compliance	The flyer shall comply with all relevant aviation regulations, ensuring a flight operation in the US.
REQ-LG-HZ-02	Ease of Maintenance	The flyer shall be designed for ease of maintenance, with accessible components and standardised parts.
REQ-LG-HZ-03	Environmental Impact	The flyer shall minimise environmental impact by using sustainable materials and energy-efficient technologies.
REQ-LG-HZ-04	Operational Flexibility	The flyer shall be capable of operating in various environments, including urban, rural, and remote areas, without requiring significant modifications.
REQ-LG-HZ-05	Modularity	The flyer shall be designed with modular components to facilitate upgrades and customisation for different mission profiles.
REQ-LG-HZ-06	Cost Efficiency	The flyer should be cost-effective to manufacture, operate, and maintain, ensuring affordability for widespread use.
REQ-LG-HZ-07	Total System Weight	The total system weight should be minimised, including all equipment used during the mission (aircraft, extra fuel/batteries, supplementary parts, tools/equipment, consumables).
REQ-LG-HZ-08	VTOL	The flyer shall take-off and land vertically.
REQ-LG-HZ-09	Operating Temperature Range	The flyer shall have an ambient temperature range of 0°C to 40°C. (The competition takes place in San Francisco in February 2027).
REQ-LG-HZ-11	Landing	The flyer shall withstand a landing of at least 5 g on different terrains.
REQ-LG-HZ-12	Stability Measure	The flyer shall remain stable on various terrains.
REQ-LG-HZ-13	LG Weight	The LGS shall have a maximum weight of 20 kg.
REQ-LG-HZ-14	LG Height	The LG shall have a minimum height of 0.5 m to prevent the fuselage from needing a high waterproof IP rating.



## **2.2. Material considerations**

The LG requires high-performance materials with exceptional specific strength and shock resistance. Experience in the industry shows that the most effective ones for LG applications are steel, titanium and aluminium alloys. Recently, Glass Fiber Reinforced Plastic (GFRP) has also been researched. Carbon Fiber Reinforced Plastic (CFRP) is not considered due to its low impact resistance, which causes it to suddenly snap; assessment difficulties, since it is difficult to identify if, for instance, delamination or fibre fracture has occurred; and galvanic corrosion problems when in contact with aluminium. [11]

Using the comparison Table A–1, where accessible aerospace-graded materials were included, the steel was discarded due to its relatively low specific strength. Then, Ti-6Al-4 and Al 7075-T6 were considered. The former has a slightly higher specific strength than the latter, but this slight difference is not enough justification for the significant price difference due to budget constraints. Hence, it was concluded that Al 7075-T6 would be used, noting that formability and weldability challenges may appear in the manufacturing.

## **2.3. Comparison of Landing Gear configurations**

Three fundamental approaches have been considered when designing the landing gear.

### **1. Four individual landing struts**

With the increasing size and mass of a UAV, the structural and functional demands of its landing gear become more significant. While small UAVs (such as quadcopters for recreational camera use) use four discrete landing struts or legs, they are not feasible for a drone of the dimensions of this project. Although being lightweight, as skids are neglected, this approach has been rejected in an early stage of the design phase, also as it is not commonly used throughout the rotorcraft industry [6].

### **2. Wheeled landing gear**

An obvious advantage of the wheeled landing gear is its ground handling behavior and its oil shock absorbers as the primary energy damper. Additionally, wheels absorb energy, reducing ground impact on the rotorcraft structure [17]. However, the heavier and more complex design, including tires, rims, braking system and shock absorbers, leads to disadvantages justifying the rejection of this concept. More components also make the system more prone to errors, which require various spare parts and additional time for maintenance.

### **3. Skid landing gear**

Due to the mentioned disadvantages of the other concepts (lack of stability, complexity and weight), the decision has been made to follow the approach of two longitudinal landing skids as they are commonly used in small passenger rotorcraft; this is also the standard in the industry Fig. A–1. The focus lies on round struts (bows) as they show the best crashworthiness behaviour thanks to their significant deflection as a leaf spring,



which absorbs the landing energy [6] and is much simpler and lightweight than a shock absorber. Furthermore, a skid LGS can adapt better to doffere. It was decided to follow the approach of two continuous bows, one in the front and one in the back, instead of four struts that are separately connected to the fuselage. This makes it easier to assemble, repair or replace damaged landing gear.

## **2.4. Static stability in slope**

Following the requirement REQ-LG-GA-07 of landing on a 12-degree slope, it is important to compute the sliding, tip-over, and pitch-over angles to ensure the stability of the flyer.

### **2.4.1. Sliding angle**

The sliding angle is given by  $\theta_{crit,slide} = \arctan(\mu)$ . For a 12-degree slope angle, a static friction coefficient  $\mu_s$  of at least 0.21 would be needed. However, it is planned to use a DIN 51130 anti-slip tape R13 [5] under the skids, which, when in contact with the carpet material of the slope, would result in a very conservative  $\mu_s$  of around 0.8, far exceeding the requirement.

### **2.4.2. Pitch over angle**

The pitch over angle is given by, when computing a moment balance,  $\theta_{crit,pitch} = \arctan(\frac{l}{h})$ , i.e., the location of the COG with respect to the tipping point P, which is where the flyer would turn around backwards. At the conservative dimensioning of a minimum fuselage half-length of  $l = 1m$ , a height of the LG of  $0.5m$  (following REQ-LG-HZ-14), and a maximum COG height at  $h = 1.4m$  (the total height of the flier, but the COG would be considerably lower since the batteries are located on the flyer's fuselage floor), the critical pitch over angle would be around a very conservative 50 degrees.

### **2.4.3. Roll over angle**

Similarly to the pitch over angle, the roll over angle is computed by  $\theta_{crit,roll} = \arctan(w/h)$ , which is for the case that the flyer lands perpendicular to the slope-increasing direction. In the same conservative situation as the pitch-over angle, the critical roll-over angle would be, for a minimum fuselage half-width of  $w = 0.75m$ , at around a still conservative 34 degrees, much greater than the required 12-degree slope angle. Hence, the sliding, tip-over, and pitch-over angles do not pose a serious challenge for design.

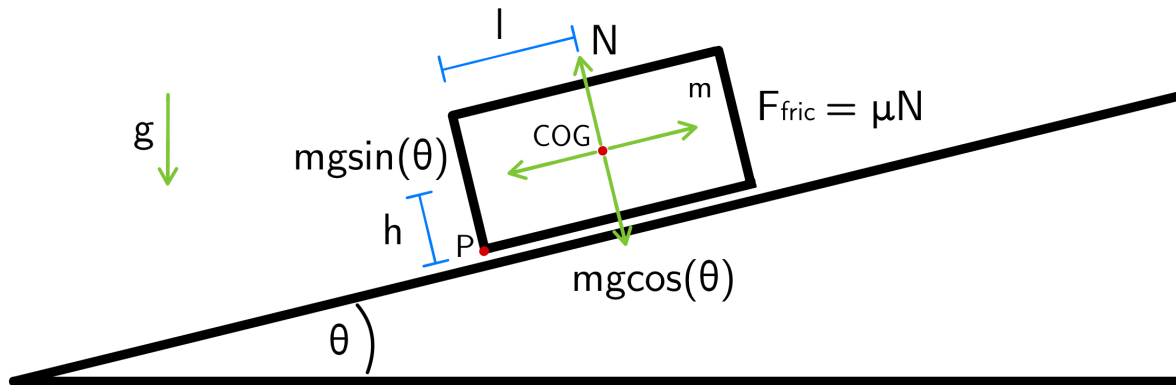


Figure 2-1.: Sketch of the static stability in slope sketch

## 2.5. Definition of Load Cases

In order to analyze deformation and internal stresses of the structure, finite element analyses have been performed using Hypermesh 2023.1 and OptiStruct. Four different load cases are considered. All assume a “hard” drop from a height of 0.46 m, corresponding to a sink rate of 3 m/s, following REQ-LG-CS27.725-15. While Load Case (LC) 1 represents the ideal case of the drone dropping straight with all skids parallel to the ground, LC2 and LC3 correspond to drops with a pitch and roll angle, respectively. LC4 is a combination of both LC2 and LC3. It is assumed that for LC2 and LC3, the total load is shared between the two respective struts that touch the ground first, meaning that the other unloaded struts remain unloaded throughout the landing process. In a real scenario, after hitting the ground with two contact points, the vehicle would rotate around the axis spanned by these very contact points and eventually land on all four struts. Hence, the approach is conservative, adding an additional safety margin and simplifying the FEA. For LC4, the entire load is applied at the one strut that touches the ground first. The horizontal position (on the x-y-plane) of the COG of the vehicle is assumed to be in the centre. For tilted landing scenarios, a conservative roll and pitch angle of 15° is assumed [12]. The total maximum occurring load is distributed over the respective struts shown in Table 2–4. For LC2-LC4, the total maximum load is split into directional components corresponding to the respective pitch or roll angle.

Table 2–4.: Overview of Load Cases

LC	Maneuver	Pitch [°]	Roll [°]	Load Distribution (percentage of load)
LC1	Ideal case	0	0	At each strut (25%)
LC2	With pitch angle	15	0	At each rear strut (50%)
LC3	With roll angle	0	15	At each left strut (50%)
LC4	Combined LC2/3	15	15	At rear left strut (100%)

## 2.6. Analysis: iteration of cross-sections and load cases

### 2.6.1. CAD model

Following the decision of the configuration for the LGS, a parametric Computer-Aided Design (CAD) model was designed with 3DExperience CATIA-V6. It comprises two skid tubes, joined to two identical bows by four connection points with bolted T-connectors. This simple, lightweight design features a thin, hollow Cross-Section (CS), allowing the system to deflect and perform as a leaf spring.

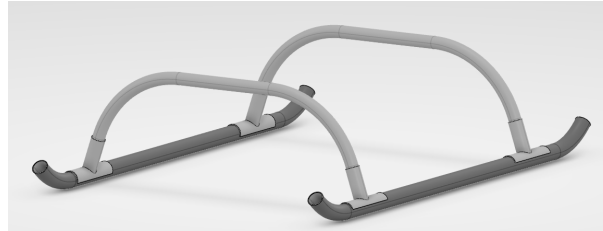


Figure 2–2.: Master Assembly of the LGS

### 2.6.2. Optimisation Process

In order to find the most suitable LGS bow geometry and CS dimensions, an optimisation process was followed under the scenario in REQ-LG-CS27.725-15. The optimisation problem, aiming to minimise the stress in the CS while keeping the transmitted load to the fuselage under the lumbar force, was set up with variables and constraints following the design requirements.

First, a list of constant design requirements was defined.

Table 2–5.: Design requirements and constants

Symbol	Magnitude	Definition	Symbol	Magnitude	Definition
$F_l$	6674 N	Max lumbar force	$\eta$	0.5 –	leaf spring efficiency
$MTOM$	380 kg	Max take-off mass	$E_{Al}$	71 700 MPa	Al Young's Modulus
$m_{LG,max}$	20 kg	Maximum LG mass	$\rho_{Al}$	$2.81 \text{ g} \cdot \text{cm}^{-3}$	Al 7075 density
$h_{drop}$	0.46 m	max drop height	$g$	$9.806 65 \text{ m} \cdot \text{s}^{-2}$	Gravitational acceleration
$l_{skid}$	2050 mm	Skid length			
$l_{bow,h}$	500 mm	Bow horizontal section where the fuselage lies			

The goal is to compute the vertical deflection, or stroke, that the bow will have at a drop test. This is due to the fact that at leaf springs, the stroke is the main driver of energy absorption. Moreover, with it, one can know how much energy is actually transmitted to the fuselage from the initial impact energy. To this end, a **list of direct input parameters** that control both the CS and the bow geometry was set up. These will be controlled by the solver, which will give values and iterate until the best solution is found.

**Table 2–6.: Direct input variables and their definitions**

Variable	Definition	Variable	Definition
$B$	Outer width of the thin box CS	$n_{ex}$	Expected load factor
$H$	Outer height of the thin box CS	$k_{abs}$	Absorbed percentage of load
$t_2$	Horizontal CS thickness	$h_{LG}$	LGS height
$t_1$	Vertical CS thickness	$\alpha$	Angle between horizontal and bow
$l_{straight}$	Length of the bow's straight section		

The solving method used to solve the optimisation problem was the Excel-implemented Generalized Reduced Gradient Nonlinear engine, which maximises or minimises an objective function by adjusting variables but subject to a **list of constraints**.

**Table 2–7.: List of constraints**

Constraint	Reason
$V_{ex} = V_{true}$	$V_{ex}$ works as a guess that, with iteration, converges to the actual true load. It is necessary because of the implicit formulation.
$A_{CS} < A_{max}$	Weight limitation.
$6 \leq n_{ex} \leq 12$	Interval of realistic g forces.
$F_{not\ absorbed} \leq F_{lumbar}$	The load transmitted to the fuselage must not exceed the lumbar force.
$B > H$	Prevention of wrong geometry.
$b, h > 0$	Prevention of wrong geometry.
$t_1, t_2 \geq 3$	Prevention of buckling or crippling.
$\alpha \geq 50^\circ > \gamma$	Prevention of very low $\alpha$ which would result in a great LGS width.
$600 \geq h_{LG} \geq 500$	Fulfillment of REQ-LG-GA-08 while keeping the COG low for static stability purposes.
$l_{straight} \geq 100 + 50$	Accommodation of the T-connector while reducing the moment at the fuselage mounting points. Plus 50 mm (approximate skid diameter) since the geometry is referenced on the ground horizontal line.

Finally, the optimisation was made possible with a set of equations of **system variables** controlled with the input variables.

**Table 2–8.: List of system variables**

System Variable	Meaning	System Variable	Meaning
$A_{CS}$	Cross-sectional area of the bow	$A_{max}$	Maximum cross-sectional area depending on mass limit
$a_{deceleration}$	Deceleration	$b$	Outer and inner width of the thin box CS

Continued on next page

Table 2–8 – continued from previous page

System Variable	Meaning	System Variable	Meaning
$F_{\text{not absorbed}}$	Force not absorbed transmitted to the fuselage	$F_s$	Reaction force in each mounting point (4 in total)
$h$	Inner height of the thin box CS	$I_{yy}$	Second moment of area about the y axis
$I_{zz}$	Second moment of area about the z-axis	$I_{yy,\text{box}}$	$I_{yy}$ of a thin box
$I_{zz,\text{box}}$	$I_{zz}$ of a thin box	$i_t$	Time to decelerate
$KE_{4 \text{ legs}}$	Kinetic energy by four landing gear legs	$KE_{\text{absorbed}}$	Kinetic energy absorbed by the system
$l_{\text{leg lever}}$	Effective lever arm of leg	$l_{\text{leg perim}}$	Perimeter of the leg, including straight and curved segments
$MTOW$	Maximum Take-Off Weight	$m_{\text{LG}}$	Actual mass of the LGS
$N_{\text{gear}}$	LG load factor, vertical deceleration rate	$n$	Load factor on gear
$n_j$	Reference load factor	$R_{\text{curved}}$	Radius of curvature for the curved section of the bow
$s$	Stroke (vertical deflection)	$V_{\text{absorbed}}$	Absorbed load by the bow
$V_{\text{ex}}$	Guess for expected vertical load	$V_{\text{true}}$	Actual real vertical impact force
$v_{\text{sink, max}}$	Maximum sink (vertical) velocity	$W_{\text{effective}}$	Effective weight
$y_{\text{curved}}$	Deflection due to the curved section of the bow	$y_{\text{straight}}$	Deflection due to the straight section of the bow
$y$	Total LGS deflection	$\sigma_{a,\text{max}}$	Maximum applied stress
$\gamma$	Angle between vertical and bow straight section		

With all this information, the iteration process that the solver follows can be clearly defined. For the sake of clarity, only the main equations are included in the following. **See Appendix A–1 and A–2 for the remaining optimisation equations completing the system.**

1. Compute the first guess of  $V_{ex}$  by varying  $n_{ex}$  and also a first guess of  $k_{abs}$ .

$$V_{ex} = MTOW \cdot n_{ex} \text{ N} \quad (2-1)$$

, where

$$MTOW = MTOM \cdot g \text{ N} \quad (2-2)$$

2. Compute the total  $KE_{4 \text{ legs}}$  applied to the 4 legs (a bow has two legs, each spanning from the T-connector until the connection point to the fuselage, i.e.,  $l_{\text{leg perim}}$ ).

$$KE_{4 \text{ legs}} = 0.5 \cdot MTOM \cdot v_{\text{sink, max}}^2 \text{ J} \quad (2-3)$$

, where

$$v_{\text{sink, max}} = \sqrt{2 \cdot h_{\text{drop}} \cdot g} \text{ m} \cdot \text{s}^{-1} \quad (2-4)$$

3. Compute  $F_s$  in each skid-bow mounting point (T-connector) using the guess from 1. [16]

$$F_s = \frac{MTOW \cdot N_{\text{gear}}}{4} \text{ N} \quad (2-5)$$

, where

$$N_{\text{gear}} = \frac{V_{\text{ex}} \cdot k_{\text{abs}}}{MTOW} \quad - \quad (2-6)$$

4. Maximise the stroke  $s$  of the bow summing the deflection of the straight part plus the curved part of the legs, which is directly dependent on the bow geometry and CS dimensions. [16] The more  $s$ , the more  $KE_{\text{absorbed}}$ .

$$s = y \cdot \sin(\gamma) \quad \text{mm} \quad (2-7)$$

$$KE_{\text{absorbed}} = \eta \cdot V_{\text{ex}} \cdot s \cdot 10^{-3} \text{ J} \quad (2-8)$$

, where

$$y = y_{\text{curved}} + y_{\text{straight}} \quad \text{mm} \quad (2-9)$$

$$y_{\text{curved}} = \frac{\pi}{4} \cdot \frac{F_s \cdot R_{\text{curve}}^3}{E_{\text{Al}} \cdot I_{yy}} \quad \text{mm} \quad (2-10)$$

$$y_{\text{straight}} = \frac{F_s \cdot \sin(\gamma) \cdot l_{\text{straight}}^3}{3 \cdot E_{\text{Al}} \cdot I_{yy}} \quad \text{mm} \quad (2-11)$$

5. The stroke is maximised by iterating the CS properties and the LGS dimensions. See A-1.
6. Compute the inertia load factor  $n$  (certification given formulas [4]) and deceleration at impact, where the stroke and drop height are considered.

$$n = n_j \cdot \frac{W_{\text{effective}}}{MTOW} \quad - \quad (2-12)$$

$$W_{\text{effective}} = MTOW \cdot \frac{h_{\text{drop}}}{h_{\text{drop}} + (s \cdot 10^{-3})} \quad \text{N} \quad (2-13)$$

$$n_j = 1 + \frac{v_{\text{sink, max}}^2}{2 \cdot g \cdot s \cdot 10^{-3}} \quad - \quad (2-14)$$

7. Compute  $V_{\text{true}}$ . It can be found with any of the following three equations, which is a conservative way to double-check that the process has no mistakes.

$$V_{\text{true}} = n \cdot MTOW = \frac{MTOM \cdot v_{\text{sink, max}}}{t_i} = \frac{KE_{4 \text{ legs}}}{s} \quad \text{N} \quad (2-15)$$

8. Compute  $F_{\text{not absorbed}}$ , which has to be below  $F_l$

$$F_{\text{not absorbed}} = V_{\text{true}} - V_{\text{absorbed}} \quad \text{N} \quad (2-16)$$

, with

$$V_{\text{absorbed}} = k_{\text{abs}} \cdot V_{\text{ex}} \quad \text{J} \quad (2-17)$$

9. Minimise  $\sigma_a$  by finding a sweet point between reducing the bow's leg lever arm  $l_{\text{leg lever}}$  while still allowing for enough deflection  $y$ .

$$\sigma_{a, \text{max}} = F_s \cdot l_{\text{leg lever}} \cdot \frac{H}{2I_{yy}} \quad \text{MPa} \quad (2-18)$$

This optimisation process was repeated in thin-box, I-beam, thin-ellipse, solid box, and circular CSs, each with different geometry parameters.  $I_{yy}$  was always relatively small to allow a maximum deflection  $y$ , whereas  $I_{zz}$  was substantially greater to easily withstand any perpendicular loading that would compromise the LGS.

The results are presented in what follows. Some deviation from the real value is expected since the static method approximates the maximum value of the dynamic landing behaviour. This allows to discard some CSs and focus on others. Further FEA will corroborate the final results.

**Table 2–9.: Maximum applied stress per CS**

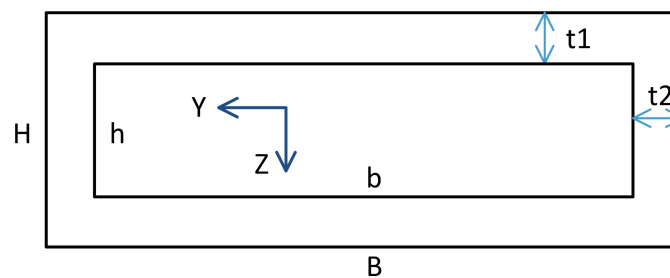
Thin Box	599,844 N	I-Beam	560,135 N
Thin Ellipse	652,034 N	Solid box	789,676 N
Circular	973,960 N		

Finally, the thin-box CS showed the best performance after the I-beam thanks to its lightweight geometry due to its thin walls, and its ability to deflect in the stroke direction by minimising the moment of inertia while preventing perpendicular motions, which explains the great width and small height. Due to issues in the FEA implementation and a lack of literature supporting the use of I-beam CS for a LGS, this CS was discarded.

The thin-box CS optimised dimensions are the following:

**Table 2–10.: thin-box CS optimised dimensions**

Variable	Magnitude	Variable	Magnitude
$B$	131.74 mm	$H$	18.35 mm
$t_1$	3 mm	$t_2$	3 mm
$k_{abs}$	79.03 %	$n_{ex}$	8.54
$\alpha$	73.00°	$h_{lg}$	500 mm
$l_{straight}$	150 mm	$R_{curve}$	503.83 mm
LGS width	1.5 m	$V_{true}$	31 831.97 N
$I_{zz}$	1 450 336.78 mm <sup>4</sup>	$I_{yy}$	48 104.28 mm <sup>4</sup>
$V_{absorbed}$	25 157.97 N	$F_{not\ absorbed}$	6674 N
$m_{LG}$	20 kg	$y_{curved}$	183.17 mm



**Figure 2–3.: Thin Box/ Thin-Walled Rectangular CS**

See Appendix A–2 for the remaining thin-box CS equations completing the system.

These dimensions were now input into the parametrised CAD and sent to HyperMesh for further FEA analysis under plenty of load cases to corroborate the design.

### 2.6.3. FEA of the optimal CAD model

The CAD model was imported into Hypermesh 2023.1 as a Standard for the Exchange of Product Data (STEP)-file. As the objective of the FEA is to analyze stresses and deformation of beams of different CSs, all beams preliminary designed with CAD were deleted and only the T-connectors were kept. Deleted beams were replaced with 1D lines and meshed with Line Mesh. For the bow, two Beam Sections (CSs) were created, namely, of the types BOX (hollow rectangle) and I (I-beam). As Beam Sections are assigned to the Line Mesh, in this way it is possible to quickly interchange (reassign) between arbitrary CSs instead of redesigning, importing and meshing the model with every change in CS. The skids were modelled with TUBE (hollow circle).

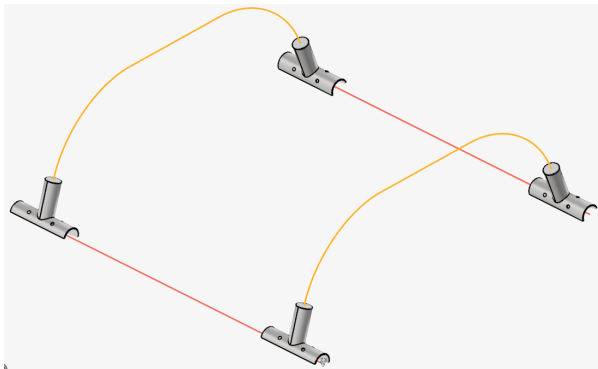


Figure 2–4.: LG Stick Model

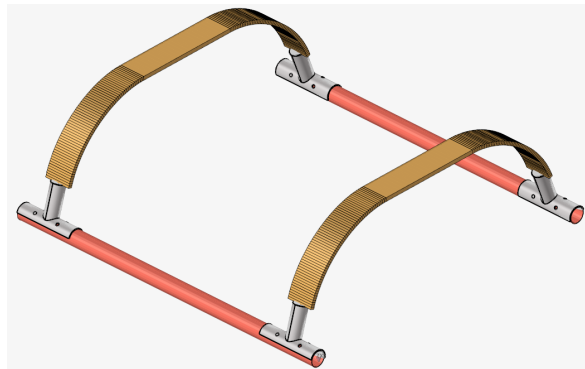


Figure 2–5.: LG Visualisation

As the T-connectors retain their circular shape in the performed FEA while the beam CS is subject to change, the connection between these two parts was simplified. Each end of the bow-line mesh was rigidly connected to the inner area of the respective T-connector using Rigid Body Element 2 (RBE2) elements. Equivalently, the skids were connected to the T-connectors in the same way.

The bow consists of one horizontal line and two round lines. The round lines are tangential to the horizontal line at one end and tangential to the T-connectors at the other end. Each connection point between the horizontal line and the round line is a constraint in the x, y, and z directions by Single Point Constraint (SPC). This way, it is assumed that the fuselage is a rigid body connected at these points with joints. The forces attack at the ends of the skid lines depending on the load case. The T-connectors are meshed as tetrahedral 3D elements. However, the focus of this work does not lie on the T-connectors and are therefore not mentioned in the interpretation.



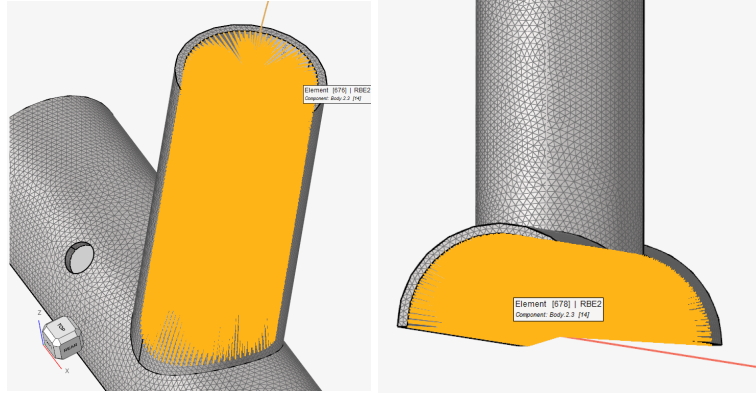


Figure 2-6.: RBE2 Element Bow    Figure 2-7.: RBE2 Element Skid

### 2.6.4. Failure Analysis

For the interpretation of the FEA, axial stresses (Element Stresses (1D):CBAR/CBEAM Axial Stress) and shear stresses (Element Stresses (1D):CBAR/CBEAM Long. Stress SBMAX) were exported. With the exported results, a strength and stability analysis is performed. Therefore, a RF is evaluated for each line mesh element. Elements with  $RF > 1$  are said to be safe [8]. For strength analysis RF is computed as follows:

$$RF_t = \frac{\sigma_{u,t,material}}{\sigma_{u,t,applied}} \quad (\text{tension}) \quad (2-19)$$

$$RF_c = \frac{\sigma_{u,c,material}}{\sigma_{u,c,applied}} \quad (\text{compression}) \quad (2-20)$$

$$RF_s = \frac{\sigma_{u,s,material}}{\sigma_{u,s,applied}} \quad (\text{Shear}) \quad (2-21)$$

For the evaluation of RF for stability, a critical stress value has to be determined. The critical stress value of a column is the lowest value of any of the four failure modes [6]:

1. Flexural instability: General column buckling dependent on end fixity, CS, and material.
2. Crippling stress: Crippling is a cross-sectional failure mode taking place after local buckling occurs in CS segments. This means, crippling is only of relevance once local buckling has occurred.
3. Interaction between local crippling and flexural instability: For critical buckling stresses reaching a value of one-half of the critical crippling stress, some interactions between flexural instability and crippling may occur.
4. Torsional instability: Failure due to torsion.

As torsion is relatively rare in columns and the interaction between local crippling and flexural instability is not relevant for certification, this work focuses on the evaluation of flexural instability and crippling stress. Slender beams primarily tend to buckling (first failure mode), whereas shorter beams tend to crippling (second failure mode). This is quantified by the column slen-

derness  $\lambda$ :

$$\lambda = \frac{cL}{r} \quad (2-22)$$

which is compared to the critical column slenderness  $\lambda_{crit}$ :

$$\lambda_{crit} = \sqrt{\frac{2\pi^2 E}{\sigma_{cutoff}}} \quad (2-23)$$

where

$$r = \sqrt{\frac{I}{A}} \quad (2-24)$$

is the radius of gyration and

$$\sigma_{cutoff} = \min(\sigma_y; \sigma_{crip}) \quad (2-25)$$

is the cutoff stress. The crippling stress is yet to be determined. The end fixity coefficient  $c$  can be read from the table presented in figure (2–8) [15].

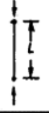
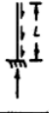

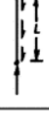
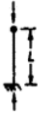



Column shape and end fixity		End fixity coefficient	Column shape and end fixity		End fixity coefficient
	Uniform column, axially loaded, pinned ends	$c = 1$ $\frac{1}{\sqrt{c}} = 1$		Uniform column, distributed axis load, one end fixed, one end free	$c = 0.794$ $\frac{1}{\sqrt{c}} = 1.12$
	Uniform column, axially loaded, fixed ends	$c = 4$ $\frac{1}{\sqrt{c}} = 0.5$		Uniform column, distributed axis load, pinned ends	$c = 1.87$ $\frac{1}{\sqrt{c}} = 0.732$
	Uniform column, axially loaded, one end fixed, one pinned end	$c = 2.05$ $\frac{1}{\sqrt{c}} = 0.7$		Uniform column, distributed axis load, fixed ends	$c = 7.5$ (Approx.) $\frac{1}{\sqrt{c}} = 0.365$
	Uniform column, axially loaded, one end fixed, one end free	$c = 0.25$ $\frac{1}{\sqrt{c}} = 2$		Uniform column, distributed axis load, one end fixed, one end pinned	$c = 6.08$ $\frac{1}{\sqrt{c}} = 0.406$

Figure 2–8.: End Fixity Coefficient

The critical stress is then calculated as follows:

$$\sigma_{crit} = \begin{cases} \sigma_{crit,Euler} = \frac{\pi^2 EI}{A(cL)^2}, & \text{for } \lambda > \lambda_{crit} \\ \sigma_{crit,Euler-johnson} = \sigma_{cutoff} - \frac{\lambda^2}{E} \left( \frac{\sigma_{cutoff}}{2\pi} \right)^2, & \text{for } \lambda < \lambda_{crit} \end{cases} \quad (2-26)$$

The RF for stability is then calculated equivalently to the strength analysis:

$$RF_{stability} = \frac{\sigma_{crit}}{\sigma_{u,c,applied}} \quad (2-27)$$

Crippling can be understood as a post-local-buckling load-carrying capability. The empirical methods used in this work consider the critical crippling stress to be greater than the critical local-buckling stress. So if the to be analyzed structure does not allow local buckling, the critical crippling stress is not relevant. On the other hand, if the structure is designed such that local buckling may occur, the crippling stress is of importance. The analyzed model in this work is assumed to allow for local buckling. Hence, the critical crippling stress is to be evaluated and is used to find  $\sigma_{cutoff}$  (2–25) [15].

### Crippling Stress of I-beams

For finding  $\sigma_{crip}$  of L-C and I-beams, the table in Figure (2–9) can be used to find  $b_i$ , which can be understood as an average width depending on the element CS and support [10].

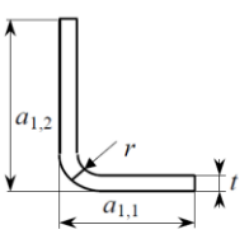
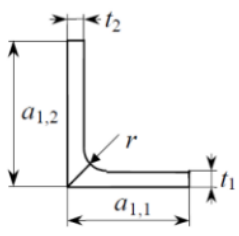
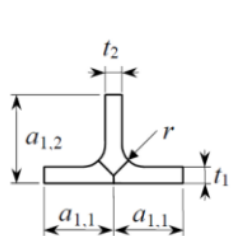
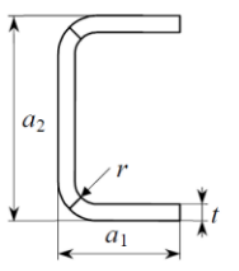
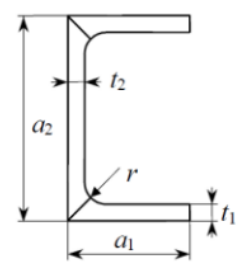
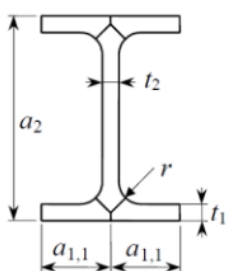
section elements			
			
elements supported at one side	$b_{1,1} = a_{1,1} - \frac{1}{2} \left( t + \frac{r}{2} \right)$ $b_{1,2} = a_{1,2} - \frac{1}{2} \left( t + \frac{r}{2} \right)$ $b_1 = a_1 - \frac{1}{2} \left( t + \frac{r}{2} \right)$ <p>(3-1)</p>	$b_{1,1} = a_{1,1} - \frac{t_2}{2} \left( 1 - 0.2 \frac{r^2}{t_1 \cdot t_2} \right)$ $b_{1,2} = a_{1,2} - \frac{t_1}{2} \left( 1 - 0.2 \frac{r^2}{t_1 \cdot t_2} \right)$ $b_1 = a_1 - \frac{t_2}{2} \left( 1 - 0.2 \frac{r^2}{t_1 \cdot t_2} \right)$ <p>(3-2)</p>	$b_{1,1} = a_{1,1} - \frac{t_2}{2} \left( 0.25 \frac{t_2}{t_1} - 0.2 \frac{r^2}{t_1 \cdot t_2} \right)$ <p>(3-3)</p> $b_{1,2} = a_{1,2} - \frac{t_1}{2} \left( 2 - 0.5 \frac{t_2}{t_1} - 0.2 \frac{r^2}{t_1 \cdot t_2} \right)$ <p>(3-4)</p>
elements supported at both sides	$b_2 = a_2 - \left( t + \frac{r}{2} \right)$ <p>(3-5)</p>	$b_2 = a_2 - t_1 \left( 1 - 0.2 \frac{r^2}{t_1 \cdot t_2} \right)$ <p>(3-6)</p>	$b_2 = a_2 - t_1 \left( 2 - 0.5 \frac{t_2}{t_1} - 0.2 \frac{r^2}{t_1 \cdot t_2} \right)$ <p>(3-7)</p>

Figure 2–9.:  $b_i$  of different cross sections

The average width  $b_i$  is plugged into (2–28)

$$x_i = \frac{b_i}{t_i} \sqrt{\frac{\sigma_y}{K_i E_c}} \quad (2-28)$$

with

$$K_i = \begin{cases} 0.41, & \text{for elements supported on one side} \\ 3.6, & \text{for elements supported on both sides.} \end{cases} \quad (2-29)$$

The stress factor  $\alpha_i$  is then

$$\alpha_i = \begin{cases} 1.4 - 0.628x_i, & \text{for } 0.4 \leq x_i \leq 1.095 \\ \frac{0.78}{x_i}, & \text{for } 1.095 < x_i \leq 1.633 \\ \frac{0.69}{x_i^{0.75}}, & \text{for } x_i > 1.633 \end{cases}$$

which is used to get the critical crippling stress of element i:

$$\sigma_{crip,i} = \alpha_i \sigma_y \quad (2-30)$$

This algorithm is to be iterated for each part of the CS. For CSs with more than one part, the critical crippling stress  $\sigma_{crip,i}$  is to be averaged over the respective area, assuming  $b_i t_i$  to be the area. The critical crippling stress is then [10]

$$\sigma_{crip} = \begin{cases} \sigma_y, & \text{for } \sigma_{crip,avg} \geq \sigma_y \\ \sigma_{crip,avg}, & \text{for } \sigma_{crip,avg} < \sigma_y \end{cases} \quad (2-31)$$

with

$$\sigma_{crip,avg} = \frac{\sum \sigma_{crip,i} b_i t_i}{\sum b_i t_i} \quad (2-32)$$

### ***Crippling Stress of Rectangular Cross Sections***

The crippling stress of each side of the thin-walled rectangular CS is

$$\sigma_{crip,i} = 0.56 \frac{\sigma_y^{0.6} E^{0.4}}{\left(\frac{b_i}{t_i}\right)^{0.8}} \quad (2-33)$$

which is to be averaged over their respective areas [3]:

$$\sigma_{crip} = \frac{\sum \sigma_{crip,i} b_i t_i}{\sum b_i t_i} \quad (2-34)$$

### 2.6.5. Application of Strength and Stability Analysis

For the analyses, the LG is subdivided into three subsections:

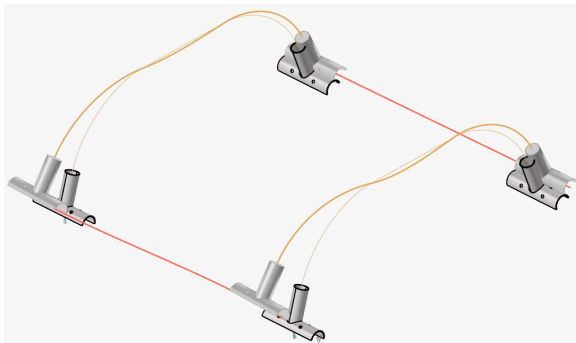
1. Horizontal section of the bow
2. Round section of the bow ("leg")
3. Skid

The theory explained in this chapter applies to straight beams. For simplicity reasons, it is also applied to the round sections. Therefore, the beam length  $L$  is assumed to be the arc length of the round "leg" section. The critical stress values for the LG presented in this work are shown in Table (2–11). As crippling does not occur in circular CSs, the critical buckling stress  $\sigma_{crit,Euler}$  serves as the critical stress for the skid.

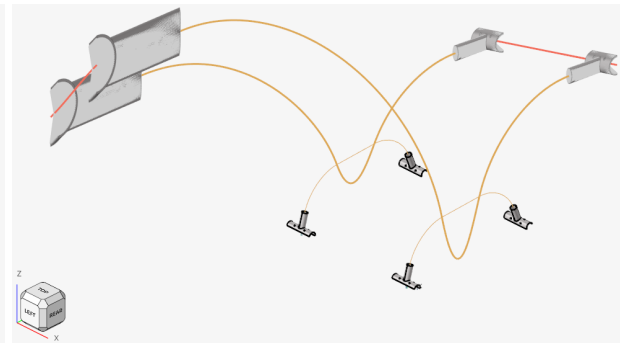
**Table 2–11.: Critical Stresses of LG Sections**

	Horizontal section	Round section	Skid
$\sigma_{crit,I-Beam}$ [MPa]	145.434	145.434	-
$\sigma_{crit,Rectangular}$ [MPa]	145.851	145.683	-
$\sigma_{crit,Hollow tube}$ [MPa]	-	-	417.561

For the considered thin-walled rectangular CS, all RFs are greater than 1. Therefore, the structure is safe. The stroke of the hollow rectangle cross section is 0.4191 m, under the LGS height and below aluminium's 7075 yield strength. The deformations shown in Figure (2–10) are moderate. For the considered I-beam, not all RFs are greater than 1. Therefore, the structure is not safe. The deformations are shown in figure (2–11).



**Figure 2–10.: Deformation, Rectangular**



**Figure 2–11.: Deformation, I-Beam**

### **2.7. Manufacturing of scaled prototype**

In collaboration with the TUM Metal Forming and Casting Chair (MFC), the opportunity to manufacture a 40% scaled prototype arose. To this end, Aluminium 7075 alloy rods were bought from a supplier, to then meet MFC staff at their workshop, where they gave valuable insight about how the forming process, the free-forming machine and post-processing software worked. Then the tubes were formed with the pre-specified dimensions. In the assembly, aluminium T-connectors off-the-shelf were used.



**Figure 2–12.: Scaled prototype**

### **3. Conclusion and Outlook**

This Engineering Project aimed to set a base and direction for the design of the landing gear of Horyzn's eVTOL participating in the GoAERO competition. After comparing three different landing gear configurations, it was decided to follow the skid type approach. Following several requirements, which set the foundation for the design, an optimisation method was developed comparing CSs. Optimizing and comparing different possible cross sections, the I-Beam and hollow rectangular were considered for further analysis. For the finite element analysis, the landing gear was simplified to a stick model to enable quick interchanging between cross sections.

The analysis of the optimized I-beam cross section shows high deflections and reserve factors smaller than one, meaning failure of the landing gear. For the optimized hollow rectangular, the analysis implies fail safe design with all reserve factors being bigger than one.

This work does not cover design and analysis of T-connectors, bolts, rivets or other fasteners and connectors which is yet to be done.

For realizing the physical landing gear, further iterative tests will have to be made and other real-life-challenges may occur, leading to possible changes of the landing gear design. Additionally, the material selection might be subject to possible change, as glass fiber reinforced plastics are considered as an alternative to aluminum at the current state of development. However, there is a lack of literature covering glass fiber reinforced land gear.



## References

- [1] A. G. Ahsaei and M. Rezaeizadeh. “FEM Analysis of Interaction Between Skid Landing Gear on the Bell 206 and Landing Surface”. In: *Engineering Failure Analysis* 117 (2020), p. 104967. DOI: 10.1016/j.engfailanal.2020.104967.
- [2] A. Airoidi and L. Lanzi. “Design of Skid Landing Gears by Means of Multibody Optimization”. In: *Journal of Aircraft* 43.2 (2006), pp. 555–563. DOI: 10.2514/1.15507.
- [3] *Astronautic Structures Manual, Volume 2*. Technical Memorandum NASA-TM-X-73306. Includes sections: NASA-TM-X-73306, NASA-TM-X-60041, NASA-TM-X-60042. Public domain document from U.S. Government. Citing Section C1.3.1. NASA, Aug. 1975. URL: <https://ntrs.nasa.gov/citations/19760071126>.
- [4] *Certification Specifications for Normal Category Rotorcraft (CS-27)*. Tech. rep. EASA CS-27 specification document. European Union Aviation Safety Agency (EASA), latest.
- [5] Deutsches Institut für Normung. *DIN 51130: Testing of floor coverings – Determination of the anti-slip properties – Workrooms and fields of activities with slip danger – Walking method – Ramp test*. <https://www.dinmedia.de/de/norm/din-51130/196898059>. Last accessed on 2025-07-05. 2014.
- [6] M. Ding, J. Cai, Y. Zhang, J. Tu, A. Xie, and D. Zhang. “Crashworthiness Analysis on Multiple Styles of Skid Landing Gear”. In: *2022 8th International Conference on Mechanical Engineering and Automation Science (ICMEAS)*. Wuhan, China, 2022, pp. 76–80. DOI: 10.1109/ICMEAS57305.2022.00023.
- [7] X. Élie-dit-Cosaque, Augustin Gakwaya, and J. Lévesque. *Design and Drop Test Simulation of a Helicopter Skid Landing Gear with Abaqus/CAE*. 2009.
- [8] Federal Aviation Administration. *14 CFR §25.301 – Loads*. Code of Federal Regulations Title 14, Part 25, Subpart C. Accessed: 2025-05-16. Federal Aviation Administration, Department of Transportation, 2024. URL: <https://www.ecfr.gov/current/title-14/part-25/subpart-C>.
- [9] *GoAero Fly-Off Rulebook version 2024-04-11*. Last accessed on 2025-07-05. URL: <https://drive.google.com/file/d/1UA83N5RbOhXYtHClvgpSt4vboTesrwg1/view>.
- [10] Industrie-Ausschuß Struktur-Berechnungsunterlagen (IASB). *Luftfahrttechnisches Handbuch (LTH): Handbuch Strukturberechnung (HSB)*. German. 3rd ed. Langzeitarchivierung durch TIB / Leibniz-Informationszentrum Technik und Naturwissenschaften und Universitätsbibliothek. München: IASB, 1969.
- [11] S. Naresh Kumar. “Design and Structural Analysis of Skid Landing Gear”. In: *International Journal of Current Engineering and Technology* 2.2 (2010), pp. 635–642. DOI: 10.14741/ijcet/spl.2.2014.121.



- [12] Benjamin L. León, Julian J. Rimoli, and Claudio V. Di Leo. “Rotorcraft Dynamic Platform Landings Using Robotic Landing Gear”. In: *Journal of Dynamic Systems, Measurement, and Control* 143.11 (Aug. 2021), p. 111006. ISSN: 0022-0434. DOI: 10.1115/1.4051751. eprint: [https://asmedigitalcollection.asme.org/dynamicsystems/article-pdf/143/11/111006/6738853/ds\\_143\\_11\\_111006.pdf](https://asmedigitalcollection.asme.org/dynamicsystems/article-pdf/143/11/111006/6738853/ds_143_11_111006.pdf). URL: <https://doi.org/10.1115/1.4051751>.
- [13] MatWeb LLC. *MatWeb: Online Materials Information Resource*. <http://www.matweb.com>. Web page. Last accessed on 2025-07-05. 2025.
- [14] S. A. Mikhaïlov, L. V. Korotkov, S. A. Alimov, and D. V. Nedel’ko. “Modeling of Landing of a Helicopter with Skid Undercarriage with Regard for the Second Landing Impact”. In: *Russian Aeronautics* 54.3 (2011), pp. 247–253. DOI: 10.3103/s1068799811030032.
- [15] Michael C. Y. Niu. *10. Column Buckling*. 1997. URL: <https://app.knovel.com/hotlink/khtml/id:kt009D27W1/airframe-stress-analysis/column-buckling>.
- [16] Daniel P. Raymer. *Aircraft Design: A Conceptual Approach*. 6th ed. Reston, Virginia: American Institute of Aeronautics and Astronautics (AIAA), 2018. ISBN: 978-1624104909.
- [17] N. Roche, M.N. Ichchou, M. Salvia, and A. Chettah. “Dynamic Damping Properties of Thermoplastic Elastomers Based on EVA and Recycled Ground Tire Rubber”. In: *Journal of Elastomers & Plastics* 43.4 (2011), pp. 317–340. DOI: 10.1177/0095244311398631. eprint: <https://doi.org/10.1177/0095244311398631>. URL: <https://doi.org/10.1177/0095244311398631>.

## A. Appendix: Additional Material

Table A–1.: Material comparison table [13]

Property	Titanium alloy Ti-6Al-4V	Aluminum alloy 7075-T6	4340 steel alloy	Units
<b>Specific strength</b>	$214.45 \cdot 10^3$	$203.56 \cdot 10^3$	$163.31 \cdot 10^3$	$\text{N} \cdot \text{m kg}^{-1}$
<b>Density</b>	4.43	2.81	7.85	$\text{g cm}^{-3}$
<b>Ultimate tensile strength</b>	950	572	1282	MPa
<b>Tensile yield strength</b>	880	503	862	MPa
Elasticity modulus	113.8	71.7	200	GPa
Poisson's ratio	0.342	0.33	0.29	-
Fatigue strength	240	159		MPa
Shear modulus	44	26.9	78	GPa
<b>Shear strength</b>	550	331		MPa
Elongation at break	14%	11%	12.2%	-

Weight vs LG type				
System Name	MTOM (kg)	LG table	Landing gear type	Landing gear weight estimation
Lilium Jet	3175	2	Tricycle LG	222,25
Archer Aviation Midnight	3175	2	Tricycle LG	222,25
Jaunt	2722	2	Tricycle LG	190,54
ALIA-250	2721	2	Tricycle LG	190,47
Bell Nexus 6HX	2720	2	Tricycle LG	190,4
Aerofugia AE200	2500	2	Tricycle LG	175
Joby Aviation S4	2404	2	Tricycle LG	168,28
CityAirbus NextGen	2200	1	Skids	154
Autoflight Prosperity 1	2000	1	Skids	140
Vahana Beta	926	1	Skids	64,82
VoloCity	900	1	Skids	63
VoloDrone	800	1	Skids	56
Grille	695	1	Skids	48,65
eHang EH216S	600	1	Skids	42
Jetson One	175	1	Skids	12,25
Jump Aero		1	Skids	0
Eve		2	Tricycle LG	0
Linx P3		2	Tricycle LG	0
VX4		2	Tricycle LG	0
Wisk Aero Generation 6		1	Skids	0

Figure A–1.: Competitor Study

**A-1. Remaining equations completing the optimisation process:**

$$\begin{aligned} \gamma &= \frac{\pi}{2} - \alpha & \text{rad} & \quad \text{(A-1a)} \\ R_{\text{curve}} &= \frac{h_{\text{LG}} - l_{\text{straight}} \cdot \sin(\alpha)}{1 - \cos(\alpha)} & \text{mm} & \quad \text{(A-1b)} \\ i_t &= \frac{v_{\text{sink, max}}}{a_{\text{deceleration}}} & \text{s} & \quad \text{(A-1c)} \\ a_{\text{deceleration}} &= \frac{v_{\text{sink, max}}^2}{2 \cdot s \cdot 10^{-3}} & \text{m} \cdot \text{s}^{-2} & \quad \text{(A-1d)} \\ l_{\text{leg lever}} &= l_{\text{leg perim}} \cdot \left( \frac{415}{650} \right) \text{ (research-based proportions)} & \text{mm} & \quad \text{(A-1e)} \\ l_{\text{leg perim}} &= l_{\text{straight}} + \frac{2\pi R_{\text{curve}}}{5} & \text{mm} & \quad \text{(A-1f)} \\ A_{\text{max}} &= \frac{m_{\text{LG, max}}}{(2 \cdot l_{\text{skid}} + 2 \cdot (l_{\text{bow, h}} + 2 \cdot l_{\text{leg perim}})) \cdot 10^{-3} \cdot \rho_{\text{Al}}} \cdot 10^6 & \text{mm}^2 & \quad \text{(A-1g)} \end{aligned}$$

**A-2. Specific thin-box cross-section equations:**

$$\begin{aligned} I_{yy, \text{thin box (CS-dependent)}} &= \frac{BH^3 - bh^3}{12} & \text{mm}^4 & \quad \text{(A-2a)} \\ I_{zz, \text{thin box}} &= \frac{HB^3 - hb^3}{12} & \text{mm}^4 & \quad \text{(A-2b)} \\ t_1 &= \frac{H - h}{2} & \text{mm} & \quad \text{(A-2c)} \\ t_2 &= \frac{B - b}{2} & \text{mm} & \quad \text{(A-2d)} \\ A_{\text{CS}} &= B \cdot H - (B - 2t_2) \cdot h & \text{mm}^2 & \quad \text{(A-2e)} \\ & & & \quad \text{(A-2f)} \end{aligned}$$